WORLD JOURNAL OF PHARMACEUTICAL RESEARCH
SJIF Impact Factor 8.084
Volume 10, Issue 13, 150-167. Review Article ISSN 2277–7105

RAMAN SPECTROSCOPY FOR STRUCTURAL FINGERPRINTING OF BIO-MOLECULES

[*1]Jimmy Alexander, [2]Arunkumar Subramanian, Dr. S. Jayaraman[3], Dr. G. Ratinavel[4]

[1]Assistant Professor, Dept. of Medicinal Chemistry, Sri Shanmugha College of Pharmacy, Tamilnadu.

[2]Research Scholar, Pharmacology.

[3]Professor, Department of Pharmacogonosy, Sri Shanmugha College of Pharmacy, Salem, Tamil Nadu.

[4]Professor, Department of Pharmaceutical Chemistry, Sri Shanmugha College of Pharmacy, Salem, Tamilnadu.

Article Received on
04 Sept. 2021,

Revised on 25 Sept. 2021,
Accepted on 15 Oct. 2021

DOI: 10.20959/wjpr202113-21302

***Corresponding Author**
Jimmy Alexander
Assistant Professor, Dept. of Medicinal Chemistry, Sri Shanmugha College of Pharmacy, Tamilnadu.

ABSTRACT

Raman spectroscopy is an increasingly popular technique in many areas including biology and medicine. It is based on Raman scattering, a phenomenon in which incident photons lose or gain energy via interactions with vibrating molecules in a sample. These energy shifts can be used to obtain information regarding molecular composition of the sample with very high accuracy. Applications of Raman spec- troscopy in the life sciences have included quantification of biomolecules, hyperspectral molecular imag- ing of cells and tissue, medical diagnosis, and others.This review briefly presents the physical origin of Raman scattering explaining the key classical and quantum mechanical concepts. Variations of the Ra- man effect will also be considered, including resonance, coherent, and enhanced Raman scattering. We discuss the molecular origins of prominent bands often found in the Raman spectra of biological samples. Finally, we examine several variations of Raman spectroscopy techniques in practice, looking at their ap plications, strengths, and challenges. This review is intended to be a starting resource for scientists new to Raman spectroscopy, providing theoretical background and practical examples as thefoundation for further study and exploration.

KEYWORDS: Raman Spectra, Raman Scattering, Major bands, Nucleic acid, Protien, Lipid.

INTRODUCTION

Raman scattering is a phenomenon in which photons incident on a sample are inelastically scattered after interacting with vibrating molecules within the sample. The effect was first discovered by Chandrasekhar Venkata Raman in 1928 for which discovery Prof. Raman received the 1930 Nobel Prize in Physics. While Raman spectroscopy is now used in biology and medicine, Raman spectroscopy found its first applications in physics and chemistry and was mainly used to study vibrations and structure of molecules. One early factor limiting the implementation of Raman spectroscopy was the weak scattering signal. Large intensities of monochromatic light are required to excite a detectable signal. This requirement became much easier to realize following the invention of the laser in 1960. Soon thereafter, lasers were used to drive Raman scattering and the number of applications increased rapidly, particularly in the analysis of biomolecules. Other important developments accelerating the progress of Raman spectroscopy include the digitization of spectra using charge-coupled devices the confocal Raman microscope, and improved filters to remove light at the laser wavelength. These inventions allowed a rapid increase in the popularity of using Raman to study biological samples in the early 1990s.

Raman spectroscopy is a popular technique in the biological sciences partially because it is non-destructive and in principle requires no sample preparation. It is therefore well-suited for applications requiring the sample to be unaltered, including *in vivo* measurements. Additionally, Raman systems operate at visible or near- infrared wavelengths can be easily integrated into standard microscopes and conventional optical fibers. Although usually a point-measurement technique, Raman spectroscopy based on laser or sample scanning can be used to create hyperspectral images. For biological samples, Raman spectroscopy is typically sensitive to concentrations of bio-molecules such as lipids, proteins, carbohydrates, and nucleic acids. Raman spectroscopy can very accurately measure relative concentrations of these molecular classes, but is poorly suited to identify specific molecules (*i.e.* specific proteins or DNA sequences). The high accuracy of Raman spectroscopy comes from detecting small changes in the relative concentrations of bio-molecules, *e.g.*, the ratio of protein to lipid within a cell or higher nucleic acid concentrations in tumour tissue. The high accuracy of Raman spectroscopy has received a great deal of attention as a potential diagnostic tool. Raman spectroscopyhas been used to classify bacteria and diagnose a broad range of diseases.

One significant shortcoming of Raman spectroscopy is the weak scattering signals from most samples. This results in long acquisition times, which can be particularly disadvantageous when creating hyperspectral images. This disadvantage can be overcome through the use of coherent Raman techniques including coherent anti- Stokes Raman scattering (CARS) and stimulated Raman scattering (SRS), which have much stronger signals than spontaneous (or incoherent) Raman scattering. This increase in signal and imaging speed comes at the expense of diverse spectral information, often acquiring signal at only one or a few wavenumbers. The low Raman scattering signal also limits the technique's ability to detect small concentrations of molecules. Surface enhanced Raman scattering (SERS) uses a metal substrate to enhance the Raman signal, making even trace amounts of molecules detectable.

$= 1.27 \times 10^4$ cm−1.

Although these units are not equivalent to energy (*e.g.*, Joules), this value is often referred to as an energy.

Quantum Mechanical Description of Raman Scattering Additional insight may be gained by considering Raman scattering through the lens of quantum mechanics. In short, this quantum mechanical treatment reveals Raman scattering as a transition between energy levels via a "virtual state." This virtual state is crucial to the phenomenon of resonance Raman scattering. Quantum mechanics will also allow us to estimate the intensities of Raman bands. Additionally, quantum mechanics allows us to understand the relative dominance of Stokes Raman scattering over anti-Stokes and derive selection rules using group theory for different molecular vibrations.

Raman Scattering as a Transition between States

Figure 2 shows various depctions of relevent scattering processes. The Jablonski energy level diagram of spontaneous Raman scat- tering in Figure 2(c) describes the process in two steps. First, the incident light drives the molecule into an excited "virtual state." This virtual state has arbitrary energy and does not have to correspond to an actual allowed state of the molecule.

Second, the molecule decays from the virtual state, releasing a photon. Most of the time depending on the temperature and distribution of states in the molecule, the molecule will

decay back into the ground state. The scattered photon will be equal in energy (and wavelength) to the incident photon. This event is called Rayleigh scattering.

Alternatively, the molecule may decay into an excited vibrational state. The scattered photon can lose energy equal to that of the vibrational state and increases in wavelength – this is Stokes Raman scattering. In anti-Stokes Raman scattering, the photon can be scattered by a molecule initially in an excited vibrational state. The scattered photon gains energy and decreases in wavelength as the molecule returns to the ground state. The quantum paths for these processes are depicted in the Feynman diagrams in Figure 2(d). The involvement of the virtual state is again apparent in this representation. Furthermore, the Feynman diagrams reveal the dependence of spontaneous Raman scat- tering on an interaction with the vacuum field. This interaction has an arbitrary phase, making the resulting scattered radiation incoherent.

Transition Rate of Raman Scattering

Fermi's Golden Rule uses quantum mechanics to provide a mathematical description of the transition rate between two states medi- ated by a transition dipole. Fermi's Golden Rule is written as

$$R|i\rangle\rightarrow|f\rangle \approx .\langle f|\mu if|i . E0| \delta(f), (15)\rangle 2| \quad 2$$

where $R|i\rangle\rightarrow|f\rangle$ is the rate of transition from initial state $|i\rangle$ to final state $|f\rangle$, μif is the perturbation of the Hamiltonian coupling $|i\rangle$ to $|f\rangle$, E0 is the electric field amplitude of the incident light, and $\delta(f)$ is the density of final states. Here, $d|i\rangle\rightarrow|f\rangle = \mu if$ E0 is the transition dipole facilitating the transition from $|i\rangle$ to $|f\rangle$. The coupling between the initial and final states of a given transition can.

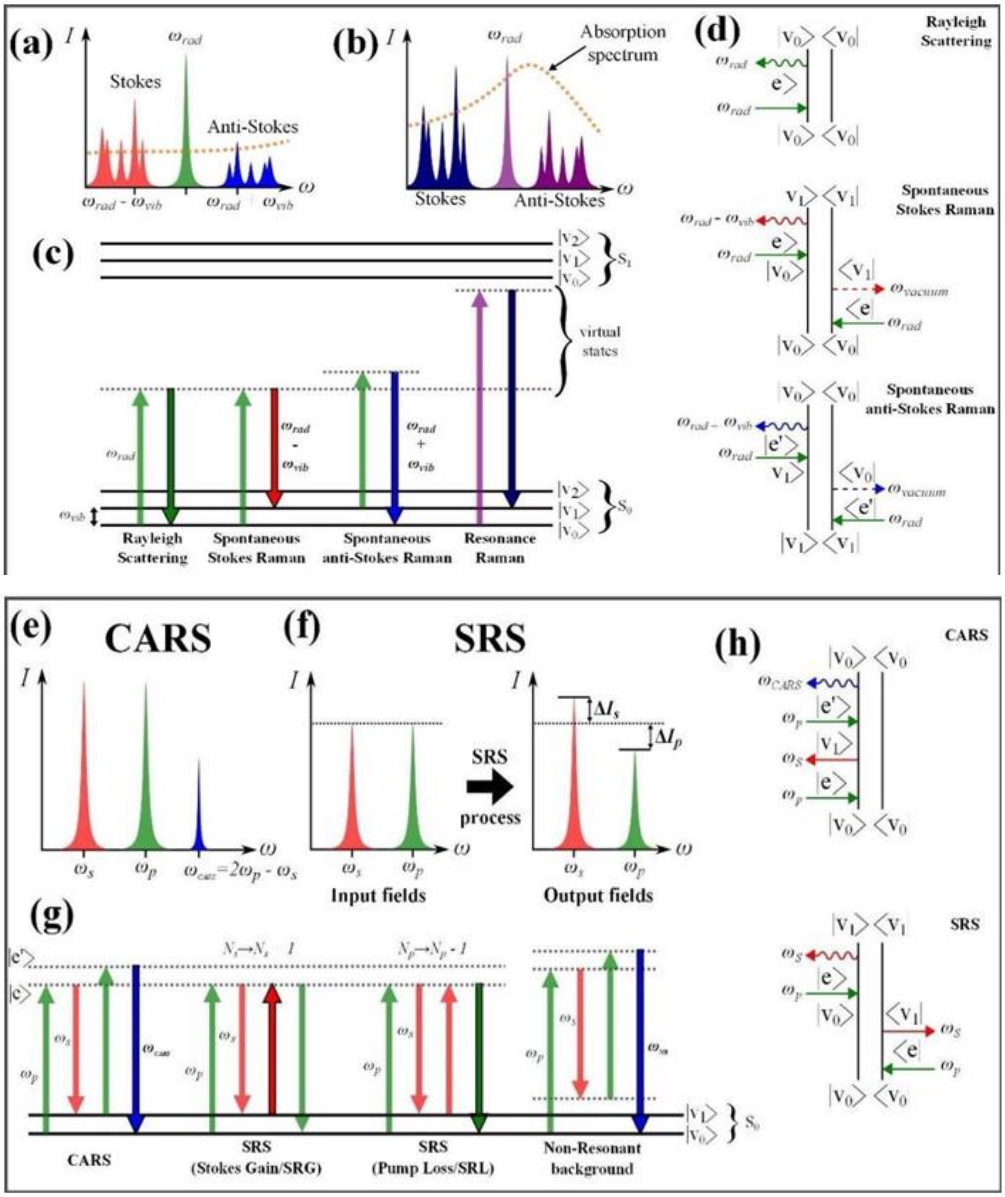

Fig. 2: Energy level, spectral, and Feynman diagrams for spontaneous and coherent Raman processes. Transition arrows with black outlines and bold labels indicate the experimentally measured feature. Spectral intensities are not to scale. Using a single excitation beam (away from absorption band) will generate weakRaman scattering at many different vibrational Stokes and anti-Stokes frequencies.

Excitation near electronic resonance (absorption band) greatly increases the scatteringsignal. Energy level diagrams for spontaneous scattering processes including Rayleigh, Stokes Raman, anti-Stokes Raman, and reso- nance Raman scattering.

Feynman diagrams for Rayleigh, Stokes Raman, and anti-Stokes Raman scattering. In the spontaneous Raman scattering processes, the *bra* state interacts with the vacuum field.

CARS utilizes pump and Stokes beams tuned to ωvib to populate the excited vibrational state, from which anti-Stokes Raman scattering is measured. Non-resonant contributions are also possible in this scheme, whereby all intermediate transitions aremedi- ated via virtual states.

SRS also uses two input beams, but no additional frequencies are generated by the SRS process. Instead, the intensity change in the pump or Stokes beam is measured. Energy level diagrams for coherent scattering processes including CARS, SRS, and nonresonant background.

Feynman diagrams for CARS and SRS. These processes are driven by coherent interactions with pump and Stokes (or probe) beams. These coherent interactions greatly increase the measurable signal.

RAMAN SPECTRA OF BIOLOGICAL MOLECULES

Many biological molecules contribute to the Raman spectra of cells and tissues. Mostcommon spectral features are caused by vibrational modes in lipid, protein, and nucleic acid molecules.

Raman spectra of biological samples are divided into three spectral regions. The fingerprint region covers the range between 600 and 1800 cm^{-1}. This region gets its name from the diversity of sharp, localized spectral features that give molecules unique "fingerprints." These molecular fingerprints can allow sample classification and chemometric analysis. Vibrations contributing bands to this region usually involve somewhat larger atoms (*e.g.*, carbon, nitrogen, oxygen) or complexes of several hydrogen atoms.

The fingerprint region of the Raman spectra of common bio-molecules is shown in Figure 7. The majority of this section will describe the most dominant components ofthese spectra in detail. Most bonds involving independently vibrating hydrogen atoms vibrate with much higher energies than other bonds. The small mass of hydrogen causes a smaller reduced mass for the whole bond. These higher energy vibrations occupy the region from 2500 to 3400 cm−1, which is known as the "high wavenumber region"of a Raman spectrum. Between the fingerprint and high wavenumber regions lies the "silent region."

This spectral region from 1800 to 2500 cm^{-1} is mostly empty of contributions from biological molecules, although there are some exceptions including alkynes. Very large,

usually non-biological atoms can contribute Raman bands in the "low wavenumber region" below 600 cm^{-1}. Any intersection of these bands with studies of biological samples will be very application dependent, so we will not provide a general treatment here.

NUCLEIC ACIDS

MOLECULAR STRUCTURE

Nucleic acids, including DNA and RNA, are present in every organism. In eukaryotes, nucleic acid is the dominant material in the cell nucleus. The structure ofa nucleic acid can be considered in two parts, the backbone and the nucleotide bases.The molecular structure of a nucleic acid backbone is shown in Figure 8(a). The difference between RNA and DNA is in the OH group shown in parentheses. This OH in RNA is replaced by an H in DNA. This structure is repeated in a chain with a nucleotide as each link. The bases attach at the location marked as B. RNA usually exists as one such chain while DNA is almost always double-stranded.

Figure 8(b) shows the structure of individual nucleotide bases. Thymine is shown bonding to its pair adenine while cytosine is shown with its pair guanine. In RNA, thymine is replaced by uracil, which differs in structure from thymine by replacingthe CH_3 in parenthesis with a single hydrogen atom. These bases attach to their respective nucleic acid backbone at the locations marked as B. Major Raman Bands.

The most prominent Raman bands originating from the backbone of nucleic acids are located near 1095 and 785 cm^{-1} see Fig- urea 7(a) . The 1095 cm^{-1} band is associated with the symmetric stretching of the PO^{-} in the backbone, as shown in Figure 9(a). The band at 785 cm^{-1} is assigned to either symmetric stretching along theO-P-O backbone see Figure 9(b) or ring breathing in the cytosine, thymine, and uracilbases.

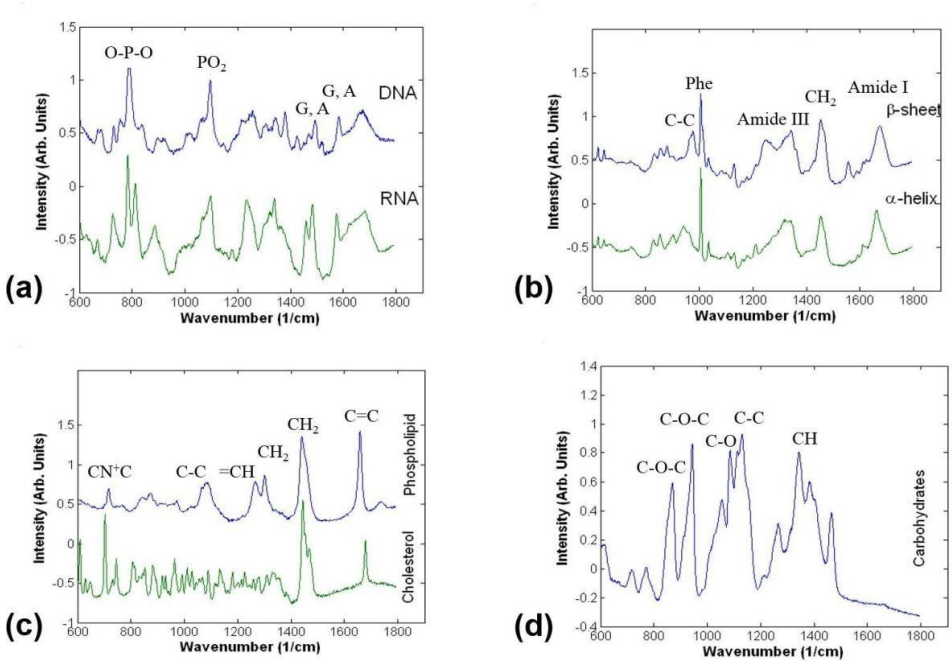

Fig. 7: Raman spectra of biological materials in the fingerprint region between 600 and 1800 cm¯1. Spectra are shifted vertically for clarity.

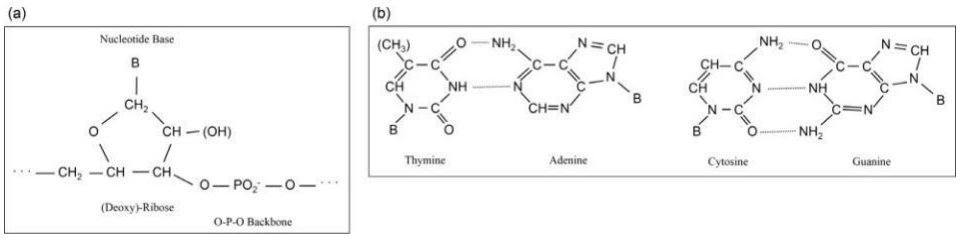

Fig. 8. (a) Structure of a nucleic acid molecule. The OH in parenthesis is only presentin RNA. It is replaced by an H in DNA. The B represents the base: adenine, thymine, guanine, cytosine, or uracil. The dots connect the CH_2 of one nulceotide to the O-P- O back- bone of the next. (b) Structure of nucleotide bases. The CH_3 in parenthesis is replaced by an H in uracil. The B represents where the base group con- nects to the nucleic acid backbone.

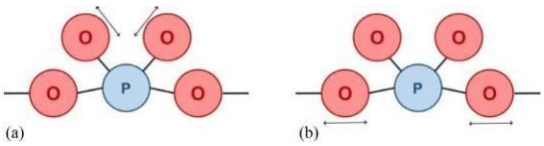

Fig. 9: Vibrational modes associated with most prominent Raman bandscorresponding to the backbone in nucleic acids.

$PO2^{-}$ symmetric stretching associated with the band near 1095 cm¯1.

O-P-O symmetric stretching often associated with the band near 785 cm¯1.

Table 3: Assignments for major Raman bands associated with nucleic acids.

Band location (cm^{-1})	Assignment	References
669	Thymine, Guanine	[69]
723-728	C-N head group in Adenine	[69–74]
763	Pyrimidines (Cytosine,Thymine, Uracil)	[74–76]
782-792	Uracil, Cytosine,Thymine ring breathing; O-P-O symmetric stretch	[69, 70, 72, 73, 76– 79]
813	RNA, A-type DNA	[77, 80, 81]
828	O-P-O	[69, 72, 73]
898	Adenine, nucleotidebackbone	[69, 70, 72]
1084-1095	PO_2 stretch	[69, 71, 77, 82, 83]
1173-1180	Cytosine, Guanine, Adenine	[79, 84, 85]
1252-1254	Cytosine, Guanine, Adenine	[69, 70, 72, 84, 86]
1304-1342	Adenine, Guanine	[69, 70, 72, 73, 78, 84, 87–91]
1369	Thymine, Adenine, Guanine	[70, 72]
1487	Guanine, Adenine	[72]
1510	Adenine	[72]
1578	Guanine, Adenine	[69, 72]
1659-1671	Thymine,Guanine,Cytosine	[70, 71, 74, 75, 77, 79, 91–97]

Table 3 lists other Raman bands originating from nucleic acids. Most of these bands are associated with vibrations of the individual nucleotide bases. Of these bands, themost visible are often the bands near 1330 and 1575 cm^{-1}, both of which are assigned to adenine and guanine.

PROTEINS

Molecular structure Proteins are responsible for a myriad of structural andfunctional roles in living systems.Every protein is assembled from chains of amino acid building blocks, of whichthere are 21 main types. All amino acids consist of a backbone unit of Cα C(= O)= N which repeats along the polypeptide, and a side-chain group attached to the alpha-Carbon (Cα), which distinguishes the amino acids from oneanother (usually denoted R).

For a chain of amino acids, the interaction between side-chain groups and the backbone determines the secondary structure, i.e. how the 1D backbone chain will be arranged and oriented. There are a several mechanisms for these interactions, as different side- chains can either be charged, polar, hydrophobic or contain certain atoms such as sulfur (for the amino acid cysteine) which can form disulfide bonds.

These interactions also usually sensitive to the solvent and pH environment which surrounds the protein. The two most common types of secondary structures in proteins are α helices and

β sheets (see Figure 10(c) and (d)), which usuallyoccur within a single protein multiple times, leading to unique higher-order "tertiary", or globular, structure.

MAJOR RAMAN BANDS

Since all proteins share the same amino-acid backbone molecular structure, they all contain a class of vibrations called the Amide modes. These modes are composed of complex combinations of motions from different parts of the backbone, and thus are not usually referred to by a specific chemical bond, but by their spectroscopic label of Amide vibrations (this terminology is shared with IR and NMR spectroscopies).

Within this class of vibrations, the Amide I and Amide III modes (see Figure 11) are the most readily observed in Raman spectroscopy (Amide II, and IV-VII are observed in IR more strongly than Raman spectroscopy, Amide A and B overlap with water bands). The relatively large range of frequencies of the Amide I and III vibrations (see Table 4) is due to the varied local molecular environment in which each backbone unit will be in due to the secondary structure. For living systems suchas cells or tissues, typically many different proteins with a mix of secondary structure will be measured in one sampling volume, resulting in broad amide bands,thus it is usually impossible to identify the presence of specific proteins directly.

Many side-chain groups have similar composition to many other biomolecules, for example the aliphatic side chains such as alanine, valine, leucine etc. The vibrations from these side-chains will typically overlap with common CH_2 and CH_3 bands in Raman spectra, making them difficult to distinguish. However, some side-chains contain molecular structures which are strongly Raman active and produce distinct bands in spectra. One of the most commonly seen is the strong sharp band due to the symmetric ring breathing mode of phenylalanine, which can usually be clearly seen in cell and tissue spectra at 1000-1006 cm−1. Other aromatic side-

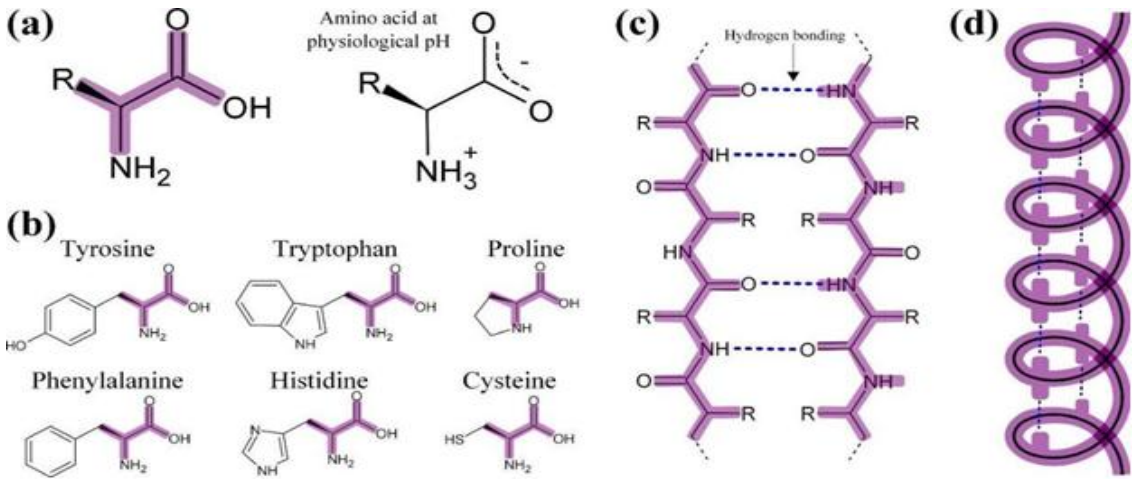

Fig. 10: (a) Generic amino acid unit, as well as its form in physiological solutions. R represents a side chain, which distinguishes a particular amino acid. The purple outline is a guide to highlight the backbone units in (b-d), which shows examples of amino acids with side-groups that contain distinguishing Raman features.

Examples of protein secondary structure: (c) *β*-sheet (anti-parallel) and (d) *α*-helix (chemical structure not shown for clarity), with hydrogen bonding between backbone chains.

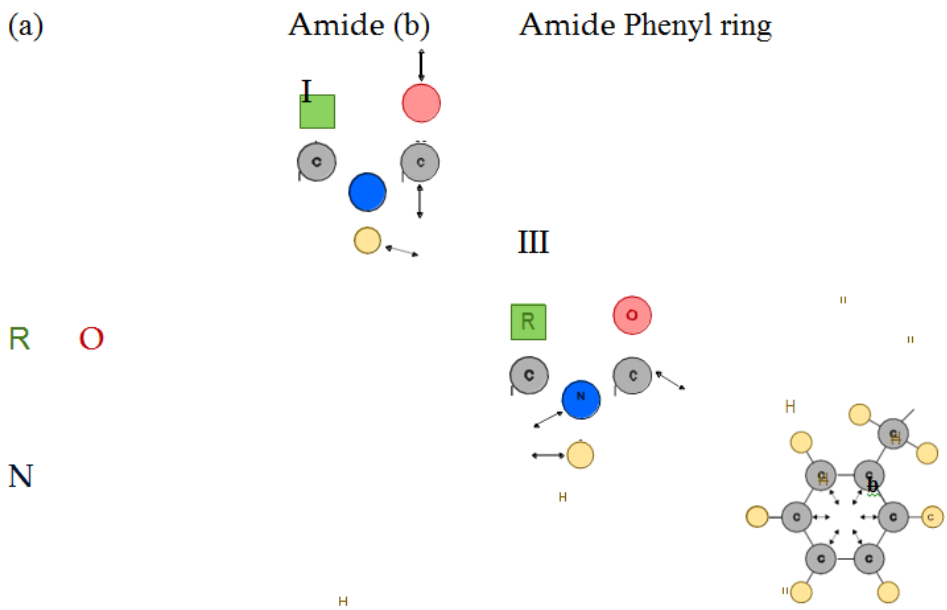

Fig. 11: Vibrational modes associated with most prominent Raman bands in proteins.

The Amide I mode at 1650-1690 cm^{-1} mostly consists of carbonyl (C=O) stretching, with a small contribution from N-H in-plane bending.

Amide III mode at 1250-1270 cm−1 has the largest contribution from the N-H mode. The sharp phenyl ring breathing mode is the most commonly observed side-chain vibration at 1000-1005 cm−1. chain groups that are visible include tryptophan and tyrosine, which has similar, butshifted, ring breathing modes to phenylalanine. Histidine and other charged side-chains are often difficult to observe in biological spectra as their conformation are sensitive to their environment, leading to variable spectra.

Methionine and cysteine are amino acids that contain sulfur atoms in their side- groups, and can thus form disulfide bridges (covalent S-S bonds) within a protein[. The corresponding S-S and C-S vibrations are seen at the lower end of the fingerprintregion, as seen in Table 4.

While we have stated that it is usually difficult to identify particular proteins using Raman spectroscopy, collagen, which is abundant in mammals as an extracellular structural component of tissue, can be an exception. This is due to the strong bandsat 850 cm^{-1} and 950 cm^{-1}, which are attributed to the proline side-group C-C stretch, which is especially abundant in collagen.

Table 4: Assignments for major Raman bands associated with proteins.

Band location (cm−1)	Assignment	References
500-550	Disulfide S-S stretch (conformationdependent)	[78, 98, 100]
755-760	Trp ring br.	[69, 78, 98, 100–102]
828-830	Tyr out of plane ring br.	[69, 78, 98, 100–103]
850-855	Pro C-C stretch (Collagen); Tyrosinering br.	[73, 101, 104];[98, 100–102]
935-937	Pro C-C stretch (Collagen); C-Cbackbone stretch (α-helix)	[73, 104]; [69, 78, 101]
1000-1006	Phe symmetric ring br.	[69, 78, 98, 100, 101, 101–103]
1014	Trp symmetric ring br.	[98, 100, 102]
1030-1033	Phe C-H in plane bend	[98, 100]
1066; 1080-1083; 1125-1128	C-N stretch	[69, 78, 101]
1155-1158	C-C / C-N stretch	[69, 101]
1170-1177	Tyr C-H in plane bend	[69, 78, 101]
1206-1214	Phe, Trp C-C6H5 stretch	[69, 78, 100, 101, 103]
1225-1280	Amide III (random coil 1225-1240; β-pleated sheet 1240-1260; α-helix 1260-1280)	[69, 78, 98, 100, 101]
1338-1340	Cα-H deformation; Trp	[69, 78, 101, 103];[100, 101]
1446-1449	C-H_2 bending	[69, 78, 101, 103]

1600-1610	Phe, Tyr C=C in plane bending	[69, 78, 100, 101, 103]
1614-1617	Tyr, Trp C=C stretch	[69, 78, 100, 101, 103]
1645-1680	Amide I (α-helix 1645-1660; β-pleatedsheet 1660-1670; random coil 1665-1680)	[98, 100, 101]

LIPIDS

MOLECULAR STRUCTURE

Another common class of molecules encountered in biological specimen are lipids. Phospholipids (lipids containing phosphate groups at their heads) are the primary molecules in membranes, including the cellular, nuclear, and mitochondrial membranes. As these membranes are present in most cells, lipids are common inevery cell type. Additionally, lipids are the dominant molecules in fatty tissue.

The basic structure of a phospholipid molecule is shown in Figure 12. The majority of the molecule consists of two long hydrocar- bon chains. These chains are typically14-24 carbons long. If all the carbon-carbon bonds in the chain are single bonds, thenthe lipid tail contains the maximum possible number of hydrogen atoms. Lipids thatare "full" of hydrogen atoms are called saturated. Unsaturated lipids contain one or more double bonds in the carbon chains.

The alcohol group at the head of the phospholipid varies in different types of molecules. The alcohol group also gives the molecule its name. The example in Figure 12 contains a choline group and is called phosphatidylcholine.

MAJOR RAMAN BANK

The Raman spectrum of a lipid molecule is dominated by the large number of bonds in the hydrocarbon chain see Figure 7(c) . The most prominent bands are located near1440 and 1650 cm−1 and associated with CH_2 scissors bending and the stretching of C=C

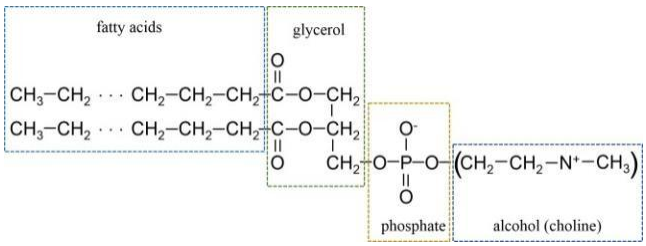

Fig. 12: Structure of a phospholipid molecule (phosphatidylcholine). The alcohol group (in parenthesis) varies. This example shows choline as the alcohol.

double bonds, respectively (see Figure 13). While the band at 1650 cm¯1 overlaps with the

Amide I protein peak, the lipid peak is generally much narrower due to the relative lack of diversity in molecular structures surrounding the C=C double bonds in the hydrocarbon chain.

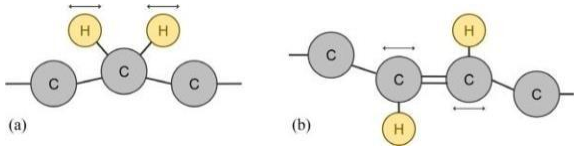

Fig. 13: Vibrational modes associated with most prominent Raman bands in lipids.

CH2 scissors bending associated with the band near 1440 cm¯1.

C=C double bond stretching associated with the band near 1650 cm¯1.

Other highly visible lipid bands are listed in Table 5. Some of these can be seen in Figure 7. Besides the CH_2 scissors and C=C bands described above, other consistently detectable bands include the CH_2 deformation band near 1300 cm¯1, the CH deformation band near 1265 cm¯1, and the C-C backbone stretches between 1030-1130 cm¯1. Various structures in the glycerol and alcohol head groups create abroad collection of bands between 840-890 cm¯1.

Table 5: Assignments for major Raman bands associated with lipids.

Band location (cm−1)	Assignment	References
719	CN+C (choline)	[105]
887	CH_2 deformations	[90]
955-975	CH_3 deformations	[73, 90, 91]
985	C-C head groups	[69]
1030-1130	skeletal C-C stretches (*cis* 1030-1040;chain *trans* 1055-1066; chain *random* 1080-1085; chain 10921098; *trans* 1127)	[69, 70, 73, 77, 90, 91, 93, 106]
1254-1284	=CH deformations	[69–72, 77]
1295-1305	CH2	[69, 70, 72, 73, 90, 91]
1310-1315	CH_3CH_2 twisting	[70, 77, 78, 85, 107]
1336-1341	CH deformations	[70, 71, 73]
1365-1380	CH_3 symmetric stretch	[69, 70, 85, 91, 108]
1440-1460	CH_2 scissors	[69, 70, 70, 71, 73, 90, 91]
1645-1660	C=C cis stretch	[69–71, 73–75, 77, 79, 91–97]
1720-1750	C=O esters	[69, 77, 91, 94, 109, 110]

FUTURE PERSPECTIVE

Technological advances during the last two decades, related in particular to lasers, detectors and optical components, have enabled the development of a broad range of Raman

spectroscopy techniques for applications in life sciences. Raman spectroscopy offers a combination of some unique features well-suited for non- destructive physical and chemical analysis of biological samples as well as noveldiagnostic tools for medical applications.

Raman spectroscopy provides high-chemical specificity without requiring labelling, which is an important feature when studying live cells. As the technique is based on light scattering, measurements can be carried out with little or no sample preparation. To obtain information regarding molecular vibrations in the sample, Raman spectroscopy uses light in the visible or near-infrared spectral regions, and thus benefits from the advanced optical microscopy and fiber optics technology. The microscopes provide high spatial resolution (0.5-1 μm) required to analyse individual cells and cellular components, while the fibre optics have enabled the development of a broad range of Raman hand-held probes and endoscopes suitable for *in vivo* medical diagnostics. In addition, Ra- man spectroscopy can also be integrated with other analytical techniques (scanning probe microscopy, electron microscopy, optical coherence tomography, etc.), and the lasers used for the excitation of Raman spectra can be used to measure the elastic scattering prop- erties of the samples or as a tool for accurate positioning and manipulation of cells (optical tweezers). Raman spectra can be easily measured of live cells in aqueous solutions (*i.e.* culture media), allowing quantification of endogenous biomolecules. The use of mul- tivariate spectral analysis techniques have enabled the development of classification models for quantitative analysis / identification of cells, as well as objective diagnosis and imaging of tissues. Nevertheless, one of the most important challenges to Raman spectroscopy in life-sciences is related to the low Raman scatter- ing cross-section of most biomolecules, leading to relatively long acquisition times (0.1-1 second per spectrum).

This limitation is particularly important when Raman spectral imaging is required at high-speed.

Another challenge is the detection of specific biomolecules within a biological sample. As all molecules excited by the laser will contribute to the Raman scattered light detected by the spectrometer, the Raman spectra of complex biological samples will consist of overlapped and convoluted bands. These overlapped bands create a background against which it is difficult to detect the signal from only specific molecules if those molecules do not possess vibrational modes that interact resonantly with the excitation wavelength. For similar reasons, many materials widely used in life sciences, such as glass microscopy slides or coverslips or

plastic cell-culture containers, are difficult to use. Instead, slides made out of quartz or more specialized materials such as calcium fluorite or magnesium fluorite are used.

Another challenge in Raman spectroscopy is the difficulty in measuring non- invasively biological samples deeper below the surface. Such measurements are of high interest, for example when investigating live cells growing in 3D cultures in- vitro or for in-vivo medical diagnosis of subsurface lesions. Although the near- infrared light used for excitation can penetrate deep into tissue, the high level of scattering reduces the signalto-noise ratio of the measured Raman spectra.

Despite these challenges, new strategies are being developed. Although none of these technologies solve every problem, specific applications can be approached using oneor more of these techniques. For example, new imaging modalities based on non- linear Raman scattering (CARS and SRS) have been developed that have demonstrated videorate imaging of cells and tissue. Additionally, selective samplingstrategies based on multimodal integration and adaptive-sampling spontaneous Raman microscopy have been designed to allow fast objective diagnosis of excised tissue specimens in cancer surgery, based on multivariate classification models. Otherapproaches relied on novel nanomaterials and photonic structures to enhance the Raman signals (SERS), allowing short mea- surements and high detection sensitivity(up to single molecule detection). These techniques also allow increased chemical specificity, as only the vibrational modes of the molecules in the vicinity (near-field) of these nanostructures are enhanced. Similar techniques can also be used for enhancing the spatial resolution down to only few nanometers (TERS). Techniques based on structured illumina- tion Raman microscopy have also been reported to increase the spatial resolution beyond the diffraction limit. Chemical specificity can also be increased by using stable-isotope labelling, which is a non-invasive technique that has allowed monitoring of molecular transfer and cell-cell communication at single live cells level. Raman labels based on small functional groups exhibiting high Raman scattering cross-sections (*e.g.*, alkynes) have also been used for monitoring cellular processes.

Significant progress has been made for *in vivo* measurements of Raman spectra at different parts of the body for medical diagnostic purposes. A broad range of fibre- optics probes have been designed to build Raman hand-held diagnostic devices and endoscopes. Improved filtering methods for the background signals have been reported; multimodal probes integrating Raman spectroscopy, tis- sue auto- fluorescence and diffuse reflectance are

currently being tested in clinical environments. Techniques based on spatially-offset and transmission Raman spectroscopy, as well as needle-probes have been developed for deep and subsurface diagnostics, as well as applications in tissue engineering and regenerative medicine. These developments have made important steps toward maximising the diagnostic accuracy and speed, and often rely on costeffective solutions that are likely to be adopted into the healthcare services. These developments demonstrate that clearly Raman spectroscopy is a powerful emerging technique in the life sciences, and has the potential to underpin fundamental advances in our understanding of molecular and cellular processes, as well as development of tools for *in vivo* disease detection and diagnosis.

REFERENCES

1. C. V. Raman and K. S. Krishnan, "A new type of secondary radiation," Nature, 1928; 121: 501–502.
2. J. H. E. t. Hibben, The Raman Effect and Its Chemical Applications (Reinhold Publishing, 1939).
3. G. Herzberg, Molecular spectra and molecular structure, vol. vol II: Infrared and Raman spectra (D. Van Nostrand Company.; New York, 1945).
4. T. Burke, D. Smith, and A. Nielsen, "The molecular structure of mof6, wf6, and uf6 from infrared and raman spectra," The Journal of Chemical Physics, 1952; 20: 447–454.
5. S. Porto and D. Wood, "Ruby optical maser as a raman source," JOSA, 1962; 52: 251– 252.
6. H. Kogelnik and S. Porto, "Continuous helium-neon red laser as a raman source," JOSA, 1963; 53: 1446–1447.
7. H. Susi and J. S. Ard, "Laser-raman spectra of lactose," Carbohydrate Research, 1974; 37: 351–354.
8. D. Rousseau, "Raman difference spectroscopy as a probe of biological molecules," Journal of Raman Spectroscopy, 1981; 10: 94–99.
9. M. Delhaye and P. Dhamelincourt, "Raman microprobe and microscope with laser excitation," Journal of Raman Spectroscopy, 1975; 3: 33–43.
10. G. Puppels, A. Huizinga, H. Krabbe, H. De Boer, G. Gijsbers, and F. De Mul, "A high-throughput raman notch filter set," Review of scientific instruments, 1990; 61: 3709–3712.
11. G. Puppels, F. De Mul, C. Otto, J. Greve, M. Robert-Nicoud, D. Arndt- Jovin, and T. Jovin, "Studying single living cells and chromosomes by confocal raman

microspectroscopy," Nature, 1990.

12. G. Puppels, H. Garritsen, G. Segers-Nolten, F. De Mul, and J. Greve, "Raman microspectroscopic approach to the study of human granulocytes." Biophysical journal, 1991; 60: 1046.
13. G. Puppels, T. B. Schut, N. Sijtsema, M. Grond, F. Maraboeuf, C. De Grauw, C. Figdor, and J. Greve, "Development and application of raman microspec- troscopic and raman imaging techniques for cell biological studies," Journal of Molecular Structure, 1995; 347: 477–483.
14. B. D. Beier, R. G. Quivey, and A. J. Berger, "Identification of different bacterial species in biofilms using confocal raman microscopy," Journal of biomedical optics, 2010; 15: 066001–066001.
15. Walter, W. Schumacher, T. Bocklitz, M. Reinicke, P. Rösch, E. Kothe, and J. Popp, "From bulk to single-cell classification of the filamentous growing streptomyces bacteria by means of raman spectroscopy," Applied spectroscopy, 2011; 65: 1116–1125.
16. O. Samek, S. Bernatová, J. Ježek, M. Šiler, M. Šery`, V. Krzyžánek, K. Hrubanová, P. Zemánek, V. Holá, and F. Ruˇ žicˇka, "Identification of individual biofilm-forming bacterial cells using raman tweezers," Journal of biomedical optics, 2015; 20: 051038–051038.
17. K. Kong, C. Kendall, N. Stone, and I. Notingher, "Raman spectroscopy for medical diagnostics - from in-vitro biofluid assays to in-vivo cancer detection," Advanced drug delivery reviews, 2015; 89: 121–134.
18. M. Diem, A. Mazur, K. Lenau, J. Schubert, B. Bird, M. Miljkovic´, C. Krafft, and J. Popp, "Molecular pathology via ir and raman spectral imaging," Journal of biophotonics, 2013; 6: 855–886.
19. C. Krafft, B. Dietzek, M. Schmitt, and J. Popp, "Raman and coherent antistokes raman scattering microspectroscopy for biomedical applications," Journal of biomedical optics, 2012; 17: 0408011–04080115.